Check for updates

Received: 13 October 2021 | Revised: 28 November 2021 | Accepted: 3 December 2021

DOI: 10.1002/cjce.24405

MINI-REVIEW

Experimental methods in chemical engineering: Scanning electron microscopy and X-ray ultra-microscopy—SEM and XuM

Thomas E. Davies[1] | **He Li**[2] | **Stéphanie Bessette**[3] | **Raynald Gauvin**[3] | **Gregory S. Patience**[2] | **Nicholas F. Dummer**[1]

[1]Max Planck–Cardiff Centre on the Fundamentals of Heterogeneous Catalysis FUNCAT, Cardiff Catalysis Institute, School of Chemistry, Cardiff University, Cardiff, UK

[2]Chemical Engineering, Polytechnique Montréal, Montréal, Québec, Canada

[3]Chemical Engineering, McGill University, Montréal, Québec, Canada

Correspondence
Nicholas F. Dummer, Max Planck–Cardiff Centre on the Fundamentals of Heterogeneous Catalysis FUNCAT, Cardiff Catalysis Institute, School of Chemistry, Cardiff University, Main Building, Park Place, Cardiff, CF10 3AT, UK.
Email: dummernf@cardiff.ac.uk

Abstract

Scanning electron microscopy (SEM) produces images at 500 000 times magnification and better than 1 nm resolution to characterize inorganic and organic solid morphology, surface topography, and crystallography. An electron beam interacts with the material and generates secondary electrons (SE) and backscattered electrons (BSE) that detectors capture. Coupled with X-ray energy-dispersive spectroscopy (X-EDS), SEM-EDS identifies elemental composition. X-ray ultra-microscopy (XuM) traverses particles to identify phase changes and areas of high density and voids without slicing through the solids by microtome. Although SEM instrument capability continuously evolves with higher magnification and better resolution, desktop SEMs are becoming standard in laboratories that require frequent imaging and lower magnification. Hand-held cameras (800–1500×) have the advantage of low cost, ease of use, and better colours. SEM depth of field is better than visible light microscopy, but image stacking software has narrowed the gap between the two. Modern user interfaces mean that today's SEM instruments are easier to operate and data acquisition is faster, but operators must be able to select the right technique for the application (e.g., SE vs. BSE). Furthermore, they must understand how operating parameters like probe current, accelerating voltage, spot-diameter, convergence angle, and working distance compromise sample integrity. The number of articles the Web of Science indexes that mention SEM has grown from 1000 in 1990 to over 40 000 in 2021. A bibliometric map identified four clusters of research: mechanical properties and microstructure; nanoparticles, composites, and graphene; antibacterial and green synthesis; and adsorption and wastewater.

KEYWORDS

electron microscopy, nanoparticles, SEM, XuM

This is an open access article under the terms of the Creative Commons Attribution License, which permits use, distribution and reproduction in any medium, provided the original work is properly cited.
© 2022 The Authors. The *Canadian Journal of Chemical Engineering* published by Wiley Periodicals LLC on behalf of Canadian Society for Chemical Engineering.

1 | INTRODUCTION

Scanning electron microscopy (SEM) has become an invaluable scientific tool to investigate the morphology of inorganic and biological materials at high magnification (1000 to – >500 000 times) and at resolutions better than 1 nm. The number of articles in Web of Science™ indexes has grown from 1000 in 1990 to 40 000 in 2020[1] and is a cornerstone of material science especially membrane technology, heterogeneous catalysis, electronics, semi-conductors, geological sciences, and biology—30% of these articles are in this scientific category. The other categories that cite SEM are applied physics (13%) physical chemistry (11%), and multidisciplinary chemistry (10%). Chemical engineering is ranked 8th with 2500 articles, and close to 10% of the articles in *The Canadian Journal of Chemical Engineering* (*Can. J. Chem. Eng.*) mention microscopy (SEM, TEM, and FESEM).

The ability to visualize the morphology of a sample with additional spectroscopic techniques such as X-ray energy-dispersive analysis (X-EDS), elemental quantification, and chemical maps is invaluable for assessing homogeneity, shape, and dimensions. The improved resolution of SEM over visible-light microscopy has been fundamental in the development of nanomaterials and advances in chemical engineering. X-ray ultra-microscopy (XuM) is an enhanced SEM method that examines the internal structure of samples without comprising the sample integrity. However, as with all microscopy, the small field of view limits the sample size that compromises determining morphological properties such as average particle size, porosity, and characteristic shape.[2] Furthermore, unlike visible light microscopy (photons), energetic electron beams require a vacuum (0.01–100 μPa) and cause sample damage and sample charging. Although modern electron microscopes are commonplace and more user-friendly than ever, only experienced practitioners get the most out of an instrument and avoid pitfalls and artefacts associated with the nature of the technique.

This tutorial review not only highlights some of these artefacts but also reviews the theory and describes some recent advances and applications that belong to a series dedicated to experimental methods in chemical engineering.[3]

2 | THEORY

2.1 | SEM electron source, column, and lenses

SEMs comprise an electron source, two or more electron lenses, a deflection system, a vacuum system, a control console, and an array of detectors that analyze the generated signals (Figure 1). The electron gun, or source, generates electrons and accelerates them to energy in the range of 0.1–30 kV. The choice of gun typically comes down to cost, lifetime, and resolution:

- Tungsten (W) wire filament sources are thermionic emitters that emit electrons as a result of resistive heating. Accordingly, they have the shortest lifetime (30–100 h) largest source size (30–100 μm), widest energy spread (1–3 eV), and lowest brightness (1×10^5 A cm^{-2} sr^{-1}), all of which ultimately lead to the lowest

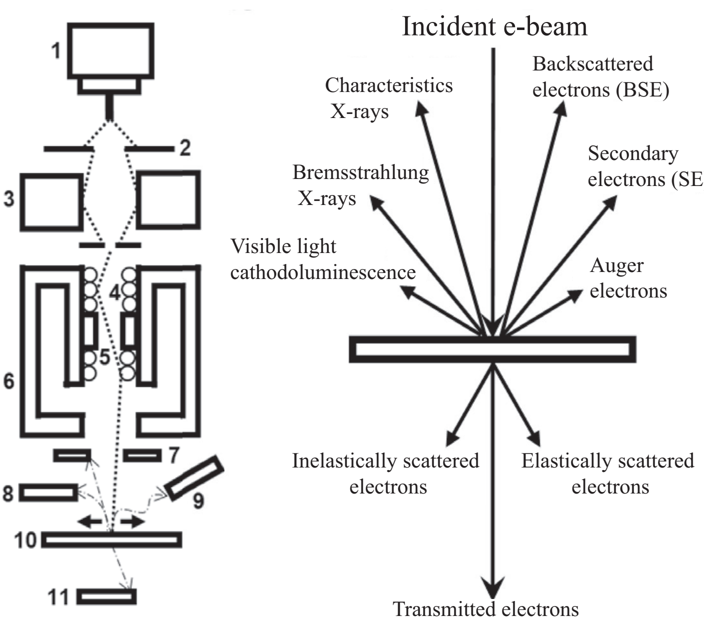

FIGURE 1 Schematic of scanning electron microscope (SEM) basic components (left panel): (1) electron gun, (2) spray aperture, (3) condenser lens, (4) deflection coils, (5) stigmator, (6) objective lens, (7) backscatter detector, (8) secondary electron detector, (9) X-ray detector, (10) sample stage, and (11) scanning transmission electron detector. Electron beam-specimen interaction (right panel)

resolution imaging. They are, however, relatively cheap, less complicated to operate and the most suitable for everyday applications.

- LaB_6 crystals are brighter (1×10^6 A cm^{-2} sr^{-1}) last longer (200–1000 h), and have a smaller spot size and energy spread, offering better resolution but at the expense of increased operating cost.
- Field-emission guns are the brightest (1×10^8 A cm^{-2} sr^{-1}), most coherent source of electrons (typically less than 1 eV), and last the longest (more than 1000 h–years). Field-emission guns come in three types: thermal, cold, or Schottky, and they are generally the best electron sources, with the only limitations being cost, stability, and the requirements for a higher vacuum.[4] Typically, a point-to-point resolution of 0.4 nm can be achieved with a cold field-emission source SEM (CFEG-SEM), but the atomic resolution is now achievable in some cases.[5]

Producing images requires the beam crossover from the source to be demagnified to a focused point or probe with a spot size <10 nm. This is achieved with electromagnetic lenses (Figure 1 left panel). The condenser lens demagnifies the beam, and the objective lens focuses the electron probe onto the sample surface (an operator-controlled function to focus the image). The objective lens also houses the stigmator, the scanning coils, and beam limiting apertures. The scanning coils are a deflection system that moves the probe in a point-by-point fashion across the surface of the sample at a certain dwell time, generating a rectangular raster. The scan generator simultaneously creates a raster on the viewing screen with the ratio of the sample raster to the image raster being the magnification. For example, a 10-μm-wide raster on the sample projected at 100 mm on a screen gives a magnification of 10 000 times. A SEM needs a vacuum system that operates from 10^{-4}–10^{-8} Pa depending on the nature of the instrument.

2.2 | Signal generation and detection

Of the nine signals that the electron beam generates (Figure 1 right panel), SEM produces images from the secondary electrons (SE) and backscattered electrons (BSE). X-ray energy-dispersive spectroscopy (EDS, EDX, or XEDS) and Auger spectroscopy identify chemical elements. The escape depths of Auger electrons are the shallowest at 1 nm, while characteristic X-rays penetrate seven orders of magnitude deeper (Figure 2). Inelastic scattering events produce SE at below 50 eV nearer the sample surface than a chamber-mounted Everhart-Thornley (ET) or an in-lens detector. The

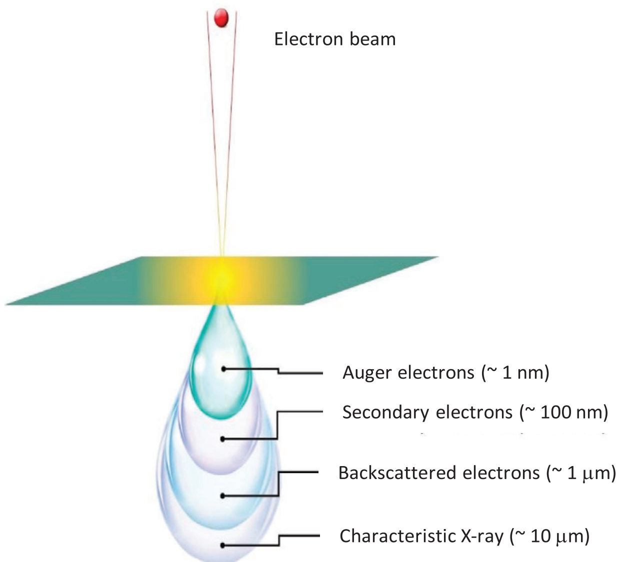

FIGURE 2 Escape depth. The actual shape and depth of the interaction volume depend on the accelerating voltage, atomic number, and tilt of the specimen surface. The escape depth of Auger electrons generated at the surface is a few nanometres. Backscattered electrons (BSE) are generated at depths a hundred times greater than secondary electrons (SE). X-rays, including characteristic X-rays, continuum X-rays, and fluorescent X-rays, are generated at the greatest depth

high resolution possible with this configuration is ideal for studying surface topography and morphology (Figure 3).

Primary electrons undergoing large-angle elastic scattering events produce BSEs (>50 eV). The BSE signal increases with atomic number (Z-contrast), which is used to distinguish between different phases and for compositional analysis (Figure 3B) as well as provide information on the topography and crystallography of the sample. Its ultimate resolution is lower than that of the secondary electron due to it being generated from a larger and deeper zone within the interaction volume (Figure 2). Secondary electrons can be of three types: SE_1 are directly generated as a result of the incident beam interaction at the beam impact point and come from the top-most portion of the interaction volume, providing the highest resolution image; SE_2 are formed as a result of multiple scattering events, typically from backscattered electrons exiting the surface away from the beam impact point; and, SE_3 are formed by the BSEs impacting on areas of the chamber such as the walls and lens system. This is important to consider when one comes to choose which detector to use for which signal. As far fewer backscattered electrons are generated compared to secondary electrons, the signal is typically weaker, especially at low probe currents. Nevertheless, when used in combination

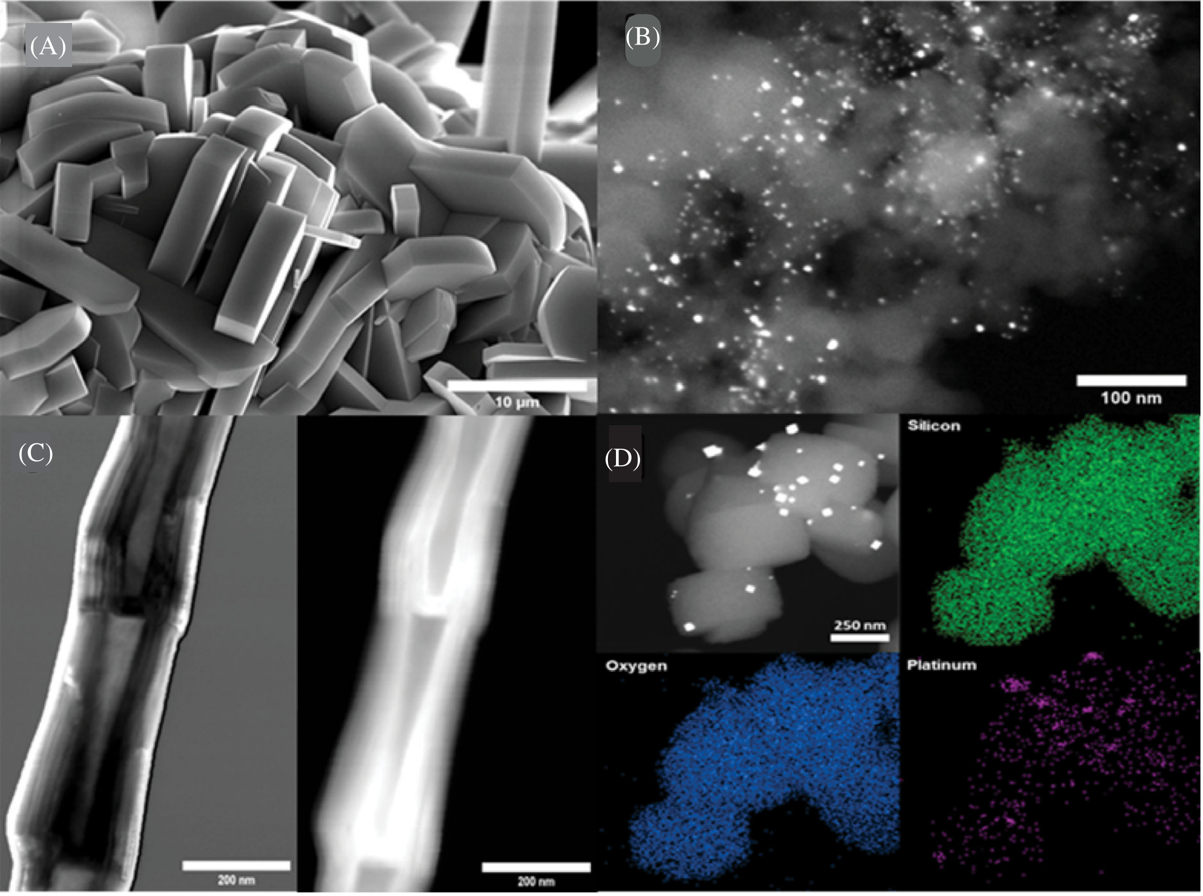

FIGURE 3 Detectors: (A) secondary electron image of silicon aluminium oxide using an in-lens secondary electrons (SE) detector; (B) backscattered electron (BSE) image of palladium nanoparticles, the particles appear as the brighter spots against the Al_2O_3 support; (C) brightfield (BF) and darkfield (DF) scanning transmission electron images of carbon nanotubes showing internal structure; and, (D) BSE image and X-ray maps of silica-supported platinum nanoparticles

with dispersive X-ray mapping, it is a powerful technique. The BSE detector is typically a retractable or fixed toroidal-type detector mounted around the pole piece but can also be in-lens.

Scanning transmission electron microscopy (STEM) in SEM is an increasingly common technique requiring a specialized holder and a brightfield (BF), darkfield (DF), and high angle annular dark-field (HAADF) detector mounted below the sample. It has limited applications due to the requirement for the samples to be thin or of a low enough density to allow the transmission of the electrons at 30 kV, but is useful for imaging the internal structure (Figure 3C). Characteristic X-rays are used for energy-dispersive X-ray analysis and provide chemical characterization due to each element having a unique X-ray emission spectrum generated upon excitation. Researchers apply the technique for the qualitative and semi-quantitative elemental point or area analysis, mapping, and line scans (Figure 3D). The primary electron loses energy by scattering and adsorption processes within the interaction volume of the specimen (Figure 2).[6,7] Excited atoms emit characteristic X-rays at greater depths within the interaction volume compared to SE or BSE, hence the typical spatial resolution of EDS in SEM is around 1–2 μm.[8] The interaction volume is variable and depends on sample density, atomic number (Z), beam energy, and sample tilt, and it can be calculated by the Monte Carlo simulation.[9]

In the case of X-ray micro-tomography (XuM) the main chamber of an SEM instrument acts as a host for the generation of X-rays, which are then directed through a suitable sample (Figure 4). The benefit of this technique is that the sample can be reconstructed in 3-D and the internal structure can be investigated without the need for sectioning.[10]

2.3 | Detectors

Most modern microscopes are fitted with a number of ports located at various positions around the sample chamber to facilitate adding multiple detectors. The

choice of detectors comes down to the requirements of the laboratory and the nature of the experiments. For standard imaging, a microscope will usually be fitted with a chamber-mounted Everhart–Thornley detector (E–T detector or ETD).[11] The ETD comprises a Faraday cage, a light guide with a metal-coated scintillator, and a photomultiplier, and is actually a combined secondary and low-energy backscattered electron detector. The Faraday cage mounted over the positively biased scintillator (10–12 kV) protects the electron beam from the high voltage and also has a bias potential applied that improves collection efficiency and is typically selectable in the range from −100 to +300 V. This means that the detector can be tuned to completely reject secondary electrons (−100 V), making it an inefficient BSE detector, or operated not only with a positive bias to efficiently collect the generated SEs but also with a low-energy BSE contribution.

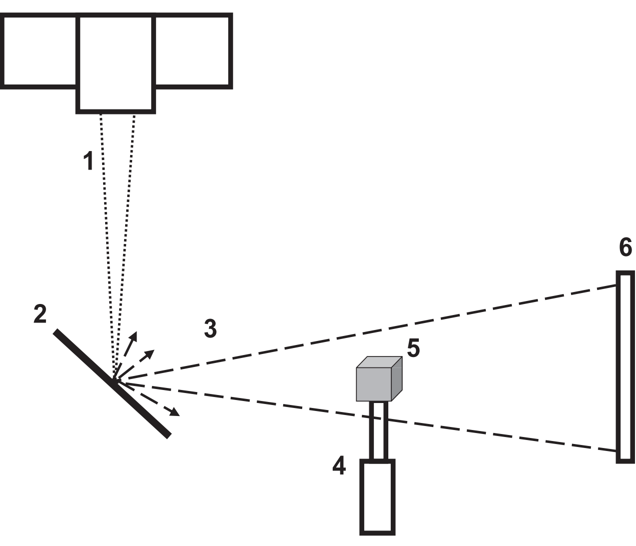

FIGURE 4 Basic X-ray ultra-microscopy (XuM) components within a scanning electron microscopy (SEM) chamber: (1) electron beam, (2) metal target, (3) X-rays, (4) sample mount, (5) sample, and (6) detector (CCD camera)

The ET detector is usually side mounted in the chamber and provides a topographic contrast image (Figures 3A and 5A) from a signal that is a mixture of SE_1, SE_2, and SE_3. An alternative SE detector is the "through-lens" or "in-lens" type that is mounted in the pole piece of the microscope and presents different information due to its location. Its position means that the highest resolutions are typically achieved using this detector as it allows for a shorter working distance and, as it primarily detects SE_1, the signal is rich in surface information as these are the electrons generated in the upper-most region of the interaction volume. Its position above the sample also means that it is "shadow" free so the image appears flatter with little topological contrast (Figure 5B).[12]

Although the ET detector can be used to detect BSEs, it is inefficient due to its off-axis location. For this reason, a dedicated annular fixed or retractable BSE detector will be located on the pole piece. This position maximizes the solid collection angle as it is located directly above the sample with the annular design permitting the primary beam to pass through the centre. The most common is the solid-state p - n junction type. As well as providing "*Z*-contrast", some annular detectors are split into four

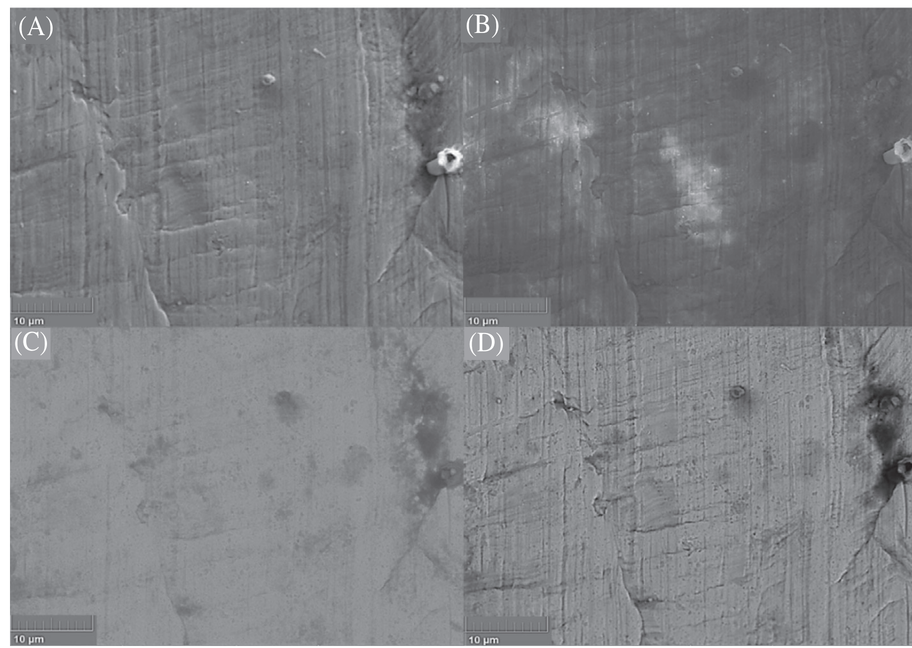

FIGURE 5 Comparison of (A) Everhart Thornley secondary electrons (SE) detector, (B) in-lens SE detector, (C) in-lens backscattered electrons (BSE) detector, and (D) in-chamber solid-state low-energy BSE (LE-BSE) detector. All micrographs are of the same area of an aluminium sample surface

quadrants that can be manipulated independently, providing topological information if only one pair of quadrants is used. Mounting a BSE detector in the lens allows for the collection of low-loss electrons that have been directly scattered from the beam interaction point. Again, this results in a higher resolution BSE image and a flatter-looking specimen due to the lack of shadowing effects (Figures 5C,D). Standard X-EDS detectors are chamber mounted and positioned to maximize the solid angle (collection efficiency). Given that detector sensitivity increases with solid angle, it is not uncommon to see dual or even quadruple EDX EDS detector systems fitted to a microscope where high sensitivity and throughput are required.

Recently, novel EDS detector designs with FlatQuad annular SDD detector permit the highest collection efficiency by inserting a retractable annular SSD device between the sample and pole piece through a horizontal port of the SEM chamber. Decreased working distance from specimen to detector combined with a high collection solid angle (up to 1 sr) and four-channel processing allows for high count rates of up to a million counts per second, with a similar detector surface area.[13] The large solid angle is beneficial for reducing the acquisition time for analyses on materials with low X-ray.[14] This annular geometry, as for annular BSE detectors, reduces shadowing effects from specimen topography and minimizes absorption of X-rays. An annular SDD EDS detector also permits analysis of materials at low energy and low probe current with a significant number of counts. Surface analysis with fewer contributions from the bulk is also made possible. The mapping of non- or semiconductive materials as well as beam-sensitive materials is greatly improved by permitting fast acquisition with low beam current settings without additional specimen preparation. Mylar polymer windows of different thicknesses protect the SSD quadrants from damage from the emitted BSEs by absorbing the BSEs and allowing the X-rays to pass through. Most standard systems will have a single detector of either the older liquid nitrogen-cooled SiLi type identifiable by the large LN_2 Dewar or the more modern Peltier-cooled silicon drift detector (SDD); the cooling is necessary to minimize electronic noise. SDD detectors offer better energy resolution, speed, and sensitivity with the performance related to the sensor size. Detector chips vary from 30–170 mm^2.[15] Windowless detectors offer higher sensitivity to low energy signals and light elements. X-EDS detectors require line-of-sight, and, for optimum analysis, the surface should be highly polished so that there is no influence of surface roughness on the signal. Where this is impractical, like in the case of powders, soft matter, or biological samples care must be taken when selecting the area of analysis. Qualitative analysis is simple and quick while quantitative analysis requires more care and time. Sample preparation, microscope parameters, data reduction, and correction for matrix effects need to be carefully considered to generate accurate and meaningful data.[4] Where overlapping peaks may be a problem, a wavelength-dispersive X-ray detector (WDS) can be used. WDS detectors separate the X-ray energies using X-ray diffraction, and although less common and more difficult to use, X-EDS offers superior resolution for finer analytical work and trace element analysis.[16] STEM in SEM can be performed using a modified sample holder fitted with a tilted reflective surface directed towards the in-chamber SE detector, however, it is now more common to see microscopes fitted with dedicated retractable brightfield (BF), darkfield (DF), and high-angle annular dark field (HAADF) detectors that can be inserted below a specialized holder. These holders usually accept the 3.05 mm carbon-coated samples grids used for transmission electron microscopy (TEM).

2.4 | SEM operation

The performance of the SEM instrument is determined by careful controlling accelerating voltage (V), probe current (i_p), probe diameter (d_p), objective aperture size or probe convergence angle (αp), and the working distance (WD) (Figure 6A). The accelerating voltage varies from <1–30 kV, and although it determines the ultimate achievable resolution due to its relationship to the electron wavelength (higher kV, shorter wavelength), it mainly affects the resulting sample interaction volume (Figure 2). Therefore, low kV operation (<5 kV) results in more surface detail, but this is usually at the expense of resolution (Figure 6C). Good practice requires systematically varying accelerating voltage on new samples to ensure adequate image quality and capture all vital surface characteristics. The probe current (i_p) is a measure of the number of electrons impinging upon the specimen surface. The high-current mode is excellent for image visibility, quality, and chemical analysis by X-EDS but the resulting larger probe diameter (d_p) will limit the resolution.

Low probe currents (small probe diameter) and slow scan speeds produce the best high-resolution images. A high i_p charge samples and damage fragile samples (low Z). To minimize beam damage, we optimize the objective aperture size, which controls the number of electrons that reach the sample and the final convergence angle (α_p). One of the key advantages of SEM compared to light microscopy is the large depth of focus, whereby more of the sample is simultaneously in focus, resulting in a

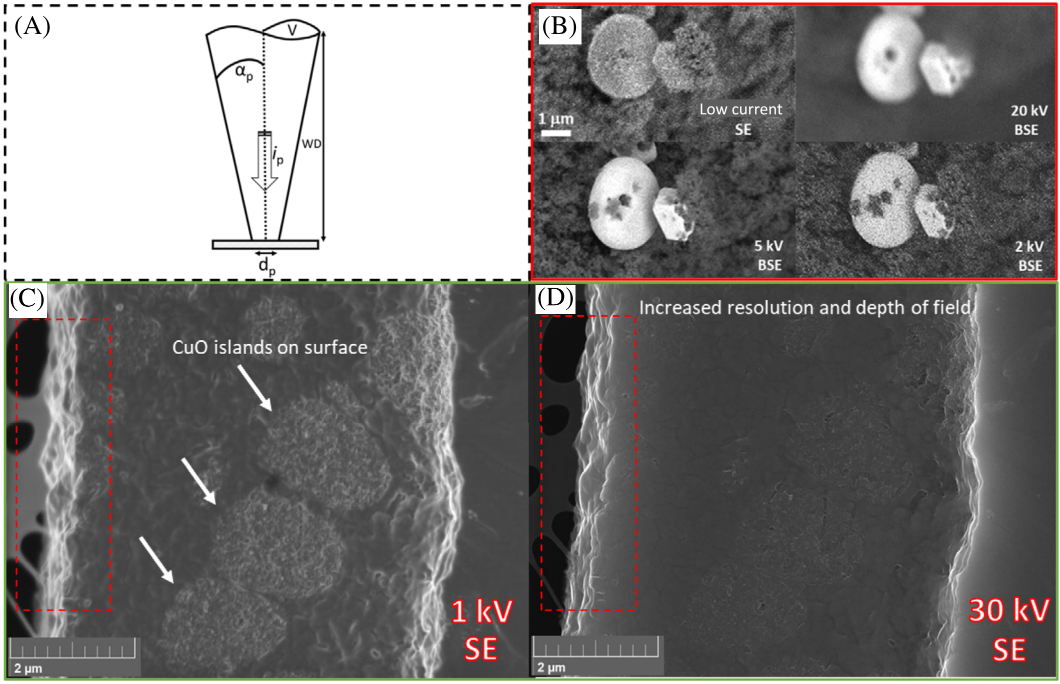

FIGURE 6 Effect of beam parameters on image modes and signal generation: (A) some of the most important parameters manipulated by the operator; (B) low-current secondary electron (SE) imaging and backscattered electron (BSE) imaging comparison at varying accelerating voltages (Au-TiO_2 catalyst); and (C) SE images at 1 kV and (D) 30 kV of copper highlighting the differences in surface detail, resolution, and depth of field as a function of kV

better three-dimensional image. Lower α_p produce a larger depth of focus. However, a lower depth of field achieved with short working distances (distance from the pole piece to the sample surface) improves resolution.

For XuM systems, electron emission guns directed towards a metal target generate X-rays. A detector at a right angle with respect to the incoming electrons records the signal (Figure 4). XuM generates microscale images of inorganic powders or aggregates, as well as wet samples such as cells or suspended particles. The contrast and signal-to-noise ratio depend on the metal foil, accelerating voltage, and beam current.[17] Moving the sample mount relative to the X-ray spot source and the detector alters the magnification. The beam parameters are intimately linked, and the optimum settings change from one sample to another.

2.5 | Sample preparation

For applications in material science sample clamps, conducting adhesives or liquid dag (a conductive mixture of processed carbon particles in a fluoroelastomer resin) secures samples to the stage. This is especially true for large bulk samples where good electrical contact is required to facilitate charge dissipation. Carbon, aluminium, and copper conductive tape, silver dag, or carbon paint adhesives ensure an adequate electrical contact. The sample must be properly secured to reduce resonant vibration while imaging. Large non-conducting samples are problematic, and when variable pressure modes are unavailable, use the thinnest or smallest sample section possible. Applying conducting coatings and resins improves image quality when charge matching or low current operation fails to produce the desired result. The chamber and the available space below the pole piece limit the maximum sample size, but typically a section or area of interest will be removed and imaged separately. Since the SEM operates under a vacuum, dry the samples first to remove moisture or residual solvent—biological samples require freeze drying, ethanol washing, and fixation with glutaraldehyde or HMDS, for example. When this is impractical, apply environmental variable pressure SEM with a cryo-stage to image samples in their native state without the introduction of artefacts. Non-conductive or poorly conductive samples such as polymers, ceramics, material fibres, glasses, minerals, plastics, and organic or biological samples are sputter coated with a highly conducting metal such as gold or evaporation-coated with carbon (other metal sources are available depending upon the application). Thin coatings maximize image quality of the surface features. Sputter coaters with turbo molecular pumps and film thickness monitors ensure that the

metal grain size and coating are tailored to match the requirements of the experiment.

Powders can be dry dispersed onto adhesive carbon tape, directly onto a metal stub or, when using STEM in SEM, can be supported on 3 mm copper grids coated with carbon film like those used for transmission electron microscopy (TEM). We remove loose particulates by tapping or carefully blowing the surface with compressed air or something similar. Loose particles contaminate the chamber or cause ballistic damage to the thin membrane of the detector windows. Sputter coating is necessary for non-conducting particulates.

Polishing with fine abrasives, chemical etching, or ion milling reduces defects and produces a flatter surface for applications like electron backscattering diffraction (EBSD) and X-EDS. Ion milling produces ultra-flat surfaces and contrast enhancement. Embedding thin films and delicate samples in resin maintains their structural morphology, particularly when imaged in cross-section. Solvent washing, UV, or plasma cleaning removes debris and contamination.[18,19]

3 | APPLICATIONS

The number of articles the Web of Science Core Collection™ has indexed with *scanning electron* as a search criterion has grown from just over 500 in 1989 to 41 200 in 2020.[1] The spectroscopic technique appears in 3700 journals and 180 of the 250 science categories in WoS Material science, physics, and chemistry are the categories that apply to SEM most. The journal *Materials* published 796 articles in 2020, and the other top journals were: *Ceramics International* (540 articles), *Journal Of Alloys And Compounds* (467), *Materials Today Proceedings* (451), and *Journal Of Materials Science Materials In Electronics* (429). The *Chemical Engineering Journal* was the top-ranked journal in chemical engineering with 113 articles.

To gauge how researchers apply SEM, we created a keyword bibliometric map of the 10 000 most cited articles of 2020 with VoSViewer open-access software (Figure 7).[20] The analysis recognized four clusters of researchers centred on mechanical properties and microstructure (red cluster), (nano)composites and fabrication (green cluster), adsorption and (waste) water (yellow cluster), and antibacterial/microbial and green synthesis (blue cluster). In 20202, *Can. J. Chem. Eng.* published 11 articles that mentioned *scanning electron* as a keyword or in the abstract. Eight of these articles were in catalysis and photocatalysis[21,22] while the other three were dedicated to waste water treatment and recovery of metals.[23] Nano-materials and nanofabrication and catalysis apply SE and BSE imaging to assess particle size,[24,25] morphology,[26,27] surface topology, porosity,[28] and phase separation. EDX measures composition, homogeneity, and purity[29–31] whereas catalyst deactivation and the effect of process conditions on materials can be evaluated in terms of poisoning,[32] particle sintering,[33] phase changes,[34] particle agglomeration, and attrition resistance.[35] In fabrication, SEM is used for product development,[36,37] quality assurance, and failure analysis.[38] The semiconductor industry applies SEM to view switches, transistors, and integrated circuits.[39] In biology and medicine, organic matter such as plants,[40] bacteria,[41] tissue sections, and cells is routinely analyzed.[42,43] The use of variable pressure SEMs along with cryo-stages means that organic materials can be analyzed in their near-native state.[44,45] In engineering and manufacturing, the mechanical properties of a material can be probed using specialized sample stages and micro manipulators to test creep, tensile strength, compression, and bending.[46,47] In situ capabilities are commonplace, with heating and cooling stages permitting testing under real conditions, and differentially pumped chambers or closed-cell holders allow for reaction or corrosion monitoring under gaseous environments.[48–50]

3.1 | SE, BSE, and X-EDS

Figures 8 and 9 demonstrate a typical application of SEM–EDX to an important class of heterogeneous catalysts. Ru-ZSM is a well-studied and industrially relevant catalyst for hydrogenation and partial oxidation reactions. Its catalytic activity depends on both the Ru loading and the available metal surface area, which is linked to the nanoparticle size, morphology, and dispersion. Figure 8 demonstrates the principal difference between secondary and backscattered electron imaging. Given that BSEs demonstrate atomic number, contrast (*Z*-contrast) where the number of backscattered electrons increases with increasing atomic number this forms the basis of a contrast mechanism whereby compositional variations can be detected as gradations of grey-scale. The lighter areas in Figure 8 are the Ru nanoparticles and the darker areas are the underlying ZSM-5 support. Figure 9 shows the spatial concentration of elements within the same Ru-ZSM sample. Ru forms relatively large clusters at the surface of the support, and careful inspection of the sodium map shows that it is largely associated with the ruthenium. The aluminium, silicon, and oxygen signals are also presented and are well dispersed at this scale, and there is no evidence of phase separation.

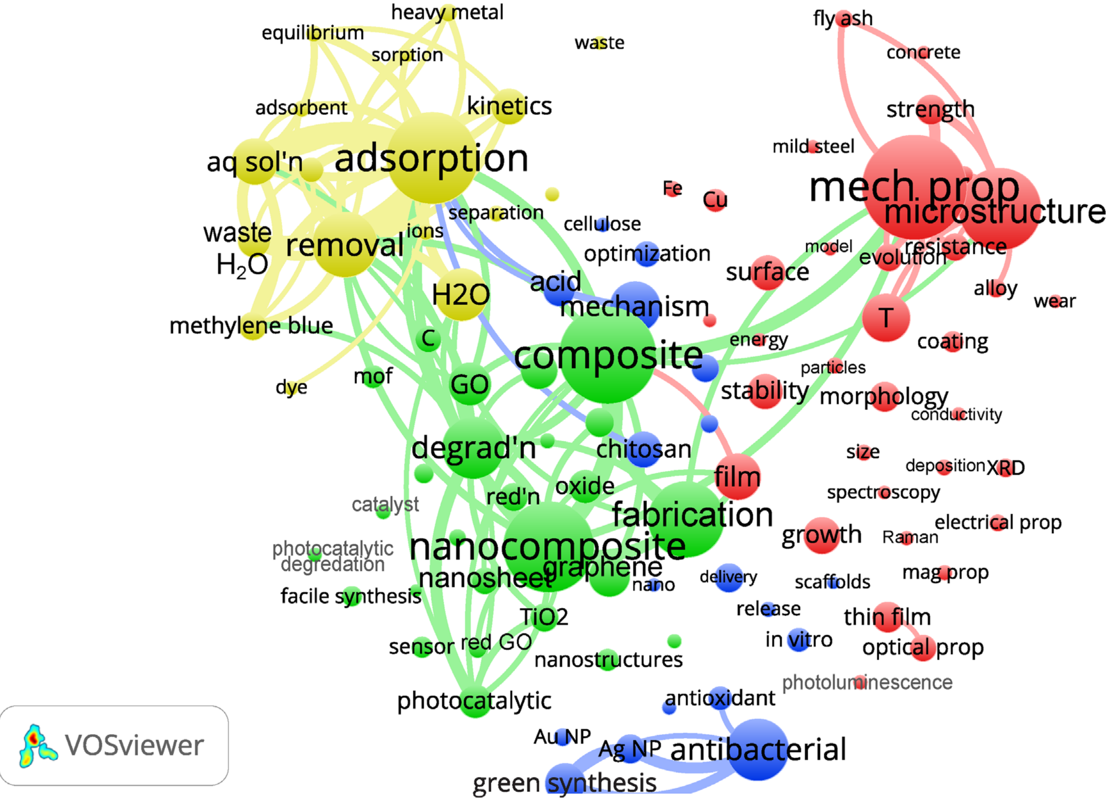

FIGURE 7 Scanning electron microscopy bibliometric map of the top 10 000 cited articles in 2020.[1,20] VOSViewer software grouped the most frequently mentioned keywords into four clusters (identified by their colour and proximity). The font and symbol size are directly proportional to the number of occurrences of the keywords in the articles: mechanical properties (mech prop) (876 articles), composites (811), antibacterial (520), and adsorption (762). The smallest circles for each category are MOF (spectroscopy, 109), supercapacitors (106) scaffolds (107), and waste (113). Lines represent citation links. We removed nanoparticles (1220 articles) and performance (1142 articles) from the map as they were very large and covered other keywords. act'd C, activated carbon; Au NP, gold nanoparticle; C, carbon; CNT, carbon nanotube; degrad'n, degradation; electrical prop, electrical properties; fabr'n, fabrication; GO, graphene oxide; magn prop, magnetic properties; mech prop, mechanical properties; MOF, metal organic framework; red GO, reduced graphene oxide; red'n, reduction; *T*, temperature; and vis light irrad, visible light irradiation

3.2 | XuM

The technique of XuM is less widespread than SEM; however, the ability to image the internal structure of suitable samples offers a unique perspective compared to techniques, which involve sectioning the sample. Samples are mounted within an SEM chamber and exposed to X-rays, rather than electrons as with SEM. As a consequence, the achievable resolution is greatly reduced in comparison to SEM, and features of interest on or within the sample must be on the micron scale. Nevertheless, we apply XuM to explore inorganic solids and even biological samples, lunar soil,[51] polymers,[52] catalysts,[53] and biological samples, and biological analogues.[54] Pakzad et al. highlighted the use of XuM as a technique to investigate the dispersion of cellulose micro-crystals in polycaprolactone as a polymer matrix.[17] Samples were reconstructed in 3D and the volume and location of the cellulose micro-crystals could be distinguished. The

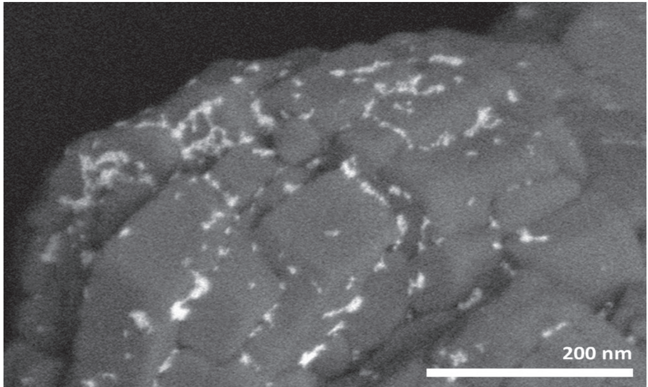

FIGURE 8 Backscattered electron image of Ru-ZSM5 catalyst demonstrating compositional contrast or Z-contrast. The lighter areas are ruthenium

benefits of such an imaging technique are tangible with respect to potentially assessing material properties such as ductility and toughness.

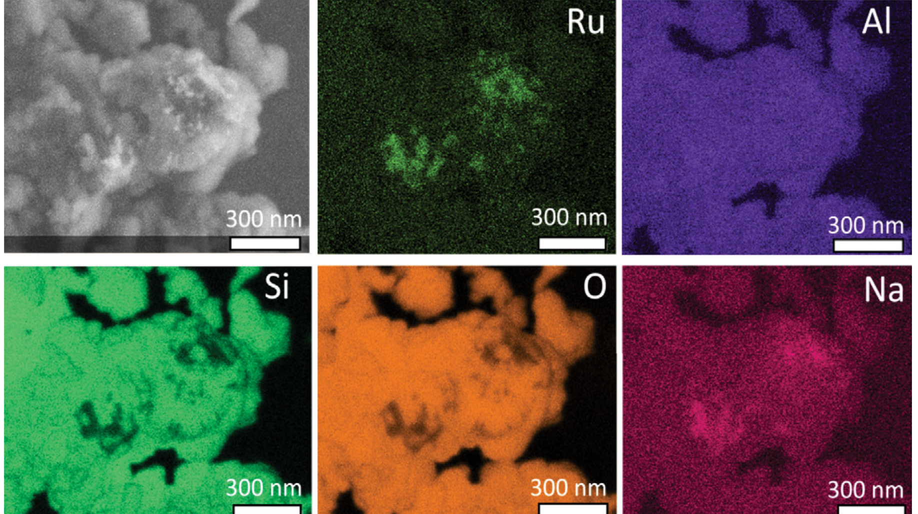

FIGURE 9 Scanning electron microscopy (SEM) and energy dispersive spectroscopy (EDS) mapping of the Ru-ZSM5 catalyst. The images are taken at 3 kV, 12 mm WD, 80 kX, and 58 min total acquisition time at 20 kcps. The Ru mapping shows the Ru spatial concentration, size, shape, and location. The Al, Si, O, and Na mapping illustrates the distribution of elements in the zeolite support

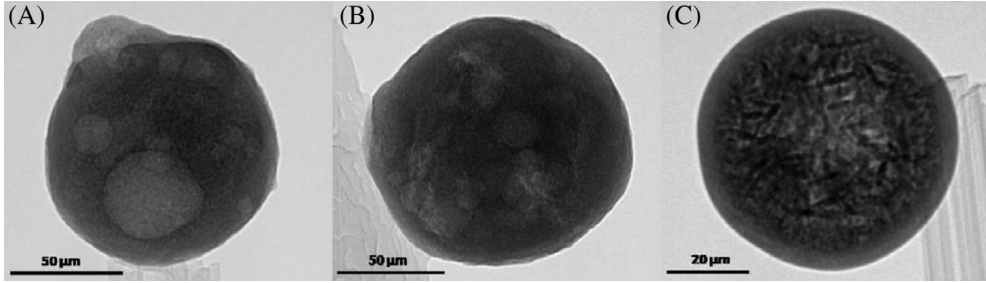

FIGURE 10 X-ray ultra-microscopy (XuM) images of vanadyl pyrophosphate (VPP) encapsulated in a silica shell; (A) precursor—vanadyl hydrogen phosphate hemihydrate, $VOHPO_4 \cdot 0.5H_2O$; (B) calcined vanadyl pyrophosphate $(VO)_2P_2O_7$) catalyst; and (C) 2-year equilibrated VPP catalyst (mixtures of vanadyl pyrophosphate and other phases). The images highlight void spaces (A and B) and phase change (C). Reproduced with permission from Dummer et al.[53] Copyright Elsevier 2010

Kiely et al. applied XuM to investigate lunar soil samples from the Sea of Tranquillity and recovered by the Apollo 11 mission.[51] The samples included several types of regolith particles, rods, teardrops, and dumbbell-shaped particles. They contrasted the SEM and XuM techniques with a glass spherule, which comprised an internal pore structure with voids and a chain of plates. The phase contrast of the particles indicated that a centrifugal force created the void spaces and dense areas. Phase contrast was applied to other particle types in combination with XEDS spot analysis, while the particle was rotated. This technique detailed the composition of the particle in 3D without sectioning.

Previously, we investigated an industrial vanadium pyrophosphate catalyst, $(VO)_2P_2O_7$, produced by spray drying a slurry of 2.4 μm platelets and polysilicic acid. During the drying process, the surface became enriched in silica and formed a hard polymeric silica 10 μm shell that improved the mechanical resistance of the microspheres that ranged from 20–200 μm (Figure 10).[53] The catalyst partially oxidized *n*-butane to maleic anhydride in the riser section of the circulating fluidized bed reactor and circulated to the air regenerator to reoxide the reduced catalyst ($V^{4+}_{riser} \rightarrow V^{5+}_{regen}$).

The spray dryer produced spherical mother particles with satellites that sheared off with time as the surface became glassy. All of the early studies on the catalyst morphology applied a microtome to slice the particles to be able to image the interior by SEM. The larger particles (70 μm) not only had circular smaller particles in the interior but also had spherical cavities. We were unsure if the cavities were produced in the microtome process that sliced the particles or they formed while drying.

XuM is non-intrusive and capable of identifying voids and areas of high density through opaque objects. Figure 10 clearly shows that the precursor and calcined catalyst have spherical voids that reach 50 μm. The underlying mechanism that produces these voids has yet to be determined. During the several years of operation in the circulating fluidized bed reactor, microscopy demonstrated that the catalyst continued to lose material and the density changed from within the silica shell structure: XuM and TEM demonstrated that the $(VO)_2P_2O_7$ phase developed two distinct $VOPO_4$. What is striking is the change in morphology from 2.4 μm flat platelets to rod-like structures that approach 10 μm.

In the case of research on biological systems, an integrated sample cell (ISC) is required to contain the specimens. She et al. built a brass tube sealed at one end with a mylar film spacer and a Ta film (at 45° to the incident electron beam) and at the other with a Mylar® film. This ISC contained red blood cells that were held in the X-ray path by a silicon nitride membrane. The red blood cells were infected with malaria, and in some cases, the parasite could be identified within the cell.[55]

As a further example of the application of the XuM technique, the second type of ISC, composed of a PTFE tube (200 μm I.D. and 100 μm thick) mounted on a Ta film 0.5 μm thick.[55] The Ta film was arranged at 45° to the incident electron, beam and the resulting X-rays passed through the sample cell and onto the detector. A suspension of polystyrene particles in distilled water was held within the PTFE tube. However, the complicated nature of the suspension was challenging to interpret and may require refinement to fully realize the benefits of observing suspended particles.

4 | LIMITATIONS

The limitation of SEM as a technique to examine materials is primarily related to sample preparation, operator expertise, cost, and the ultimate achievable resolution.[56] The high-energy ionizing electron beam can alter the sample due to knock-on damage, radiolysis, and heating so that the user must consider the beam energy, scan rate, and overall exposure time (Figure 11A,B). Non-conductive or beam-sensitive samples require the addition of a conducting layer of gold or carbon by sputter coating, which introduces artefacts. Although the effects of extreme sample charging make this a necessity to remove instances of beam instability, leading to "clipping" or streaking in the images or a "hall of mirrors" effect where the beam is completely deflected away from the surfaces, resulting in a totally distorted image (Figure 11C,D).

Samples must be robust under high vacuum so biological or wet samples are problematic, although advances in environmental or variable pressure scanning electron microscopy (E-SEM and VP-SEM) mean that imaging of samples in their natural state is becoming more routine (Figure 11E,F). Coupling this with cooling or cryo-stages means that hydrated samples can be viewed in pristine condition. Furthermore, the introduction of gas to the sample chamber results in the neutralization of negative surface charge due to electron-gas interaction, generating positive ions. Therefore, non-conducting samples can be imaged without pre-treatment or coating. The effect is achieved through the addition of pressure-limiting apertures between the chamber and column in conjunction with differential pumping. Dedicated systems such as E-SEMs can achieve pressures as high as 3000 Pa, whereas standard SEMs will offer the option of a VP mode, which can achieve pressures of up to 600 Pa. The principal drawback is the loss of resolution and increased signal-to-noise as a result of electron scattering, but improvements in detector technology mean that dedicated gaseous secondary electron detectors such as those incorporating their own turbo-pumps improve signal quality. Griffin[57] reviewed imaging of biological samples with E-SEM and VP-SEM. Ancillary equipment such as sputter coaters, plasma cleaners, ion mills, drilling, cutting, and vibratory polishers are required to embed, freeze-dry, section, thin, polish, or mill samples. For ultra-high resolution work, it is necessary to align the SEM frequently to avoid image artefacts and resolution limitations such as astigmatism due to a poorly shaped probe. When resolution becomes the limiting factor, one will employ complementary techniques such as transmission electron microscopy (TEM).[58] Ultimately, one of the major limiting factors is equipment and operational costs. Although affordable benchtop SEMs are now commonplace for routine analysis, advanced microscope designs continue to strive for higher resolution and greater capability, and with that comes an increased cost. For highly sensitive microscopes, one needs to mitigate against sources of external interference such as vibration, electromagnetic radiation, temperature changes, and acoustic noise, which requires a careful design of the environment.

In the case of XuM, the limitations are based on resolution and sample suitability. Features of interest should be on a micrometre scale. Mounting samples may require additional considerations. Larger particulate samples can be mounted on a carbon pin, which can be manipulated into position to allow the X-rays to pass through the sample. Smaller samples or biological ones may require more advanced mounting in the form of an integrated sample cell.

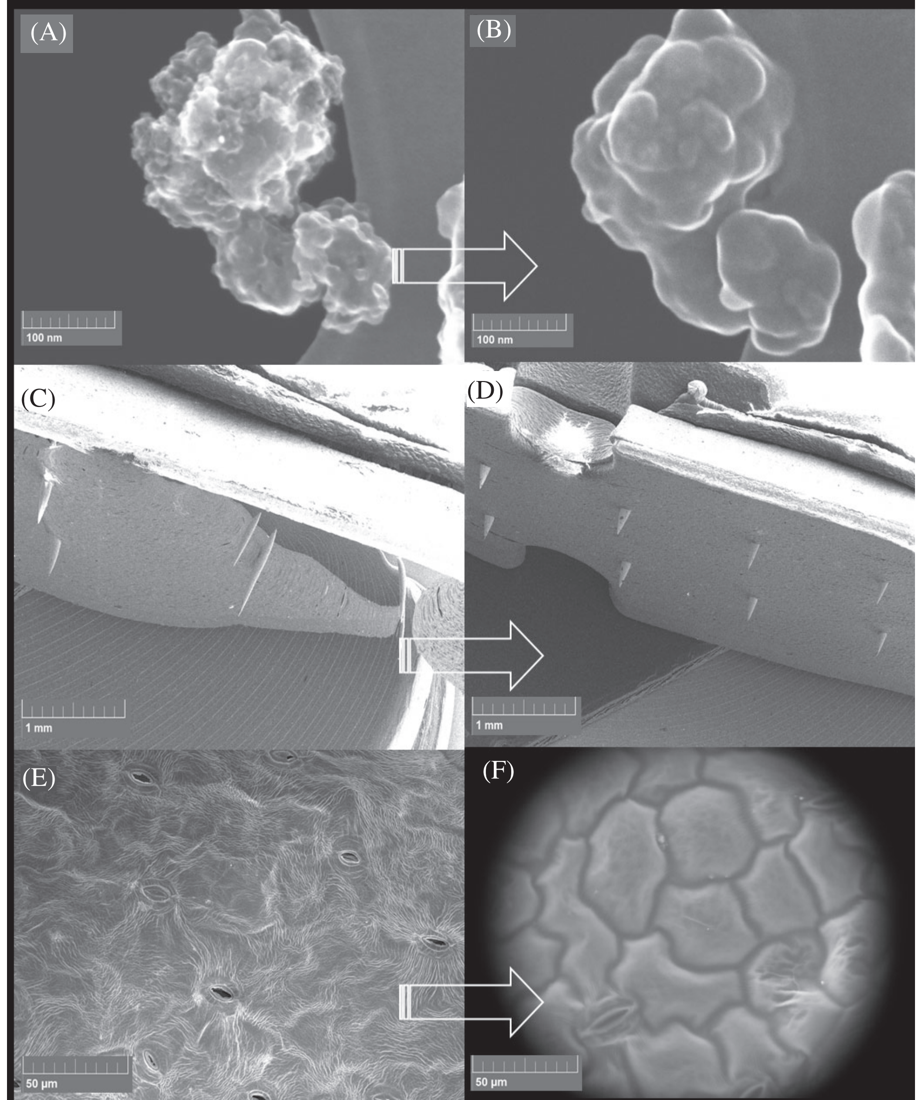

FIGURE 11 Examples of artefacts and limitations in scanning electron microscopy (SEM). Beam damage: (A) secondary electrons (SE) image of fresh carbon sample imaged for 2 min with 100 pA probe current and; (B) carbon after 2 min in a 100 pA beam. Charging: (C) polymer needle used for drug delivery imaged uncoated and (D) polymer needles imaged after coating with 25 nm Au:Pd (80:20). Vacuum damage: (E) coriander leaf imaged under typical EM vacuum conditions and (F) imaged under variable pressure scanning electron microscopy (VP-SEM) (300 Pa, −25°C)

5 | OPTICAL MICROSCOPY VERSUS SEM

The wavelength of light at 400–700 nm limits the magnification of optical microscopes to not more than 1500× and a resolution of 200 nm. SEM reaches a magnification of 500 000× with a resolution of better than 1 nm as the lower limit of X-ray wavelengths is 0.01 nm. Furthermore, the depth of focus on an SEM is much better than optical microscopy. Coupled with EDX, a SEM identifies elemental distribution while backscatter detectors and secondary electron detectors produce chemical contrast images. However, preparing samples for SEM and the instrument itself can alter their morphology. Crack propagation of moisture-sensitive cements is an example. Secondary microcracks that form while the samples dry for SEM analysis confound the analysis of the primary microcracks of interest.

The spatial resolution of several nanometres is necessary to identify structural changes in catalysts and localized carbon whiskers, for example, but for asperities, surface roughness, and larger whiskers, 200 nm resolution is good enough. Furthermore, on-line image stacking software (e.g., www.picolay.de) improves the depth of field to produce images with large populations of particles. Portable digital microscopes are capable of producing reasonable images rapidly at a fraction of the cost of an SEM. The real advantage is being able to easily identify large changes in the surface structure and colour. Vanadium pyrophosphate catalyst, for example, is mostly green after calcining the precursor (Figure 12). It becomes a dark brownish colour after years in a circulating fluidized bed reactor (Figure 13).[59] Conventional thinking attributed the colour change to smaller particles that turned black due to thermal excursions at oxygen spargers and combustion downstream of the stripper and

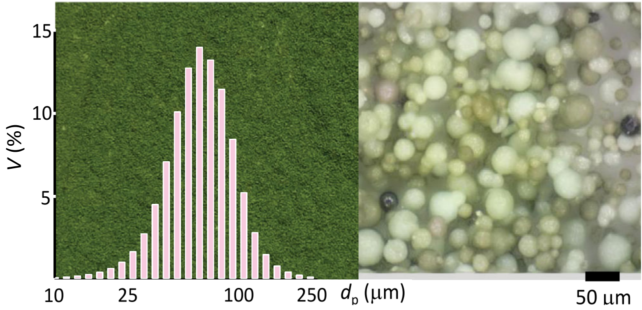

FIGURE 12 Calcined vanadyl pyrophosphate (VPP) catalyst. The image to the left is a bar chart of the VPP particle size distribution, superimposed on an optical photo of the VPP ($d_p > 45 \mu m$). The image to the left was created by image stacking with a microscope at a magnification of 830× ($d_p > 45 \mu m$)

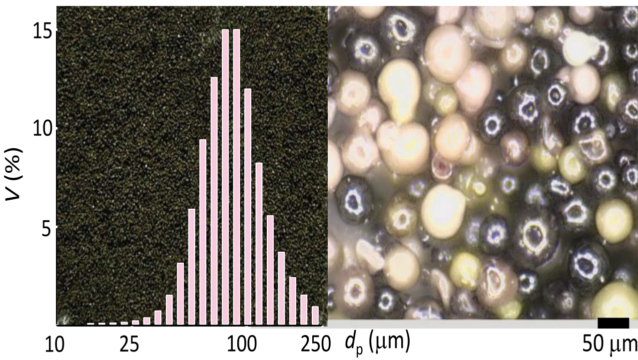

FIGURE 13 Equilibrated vanadyl pyrophosphate (VPP) catalyst. The image to the right is a bar chart of the equilibrated VPP superimposed on an optical photo of the catalyst ($d_p > 90 \mu m$). The image to the right is a stack of four images of equilibrated VPP at a magnification of 830× ($d_p > 90 \mu m$), and it was created with www.picolay.de

cyclone. The image shows that the equilibrated catalyst becomes shiny, so shiny that the circle of dots of light illuminating the catalyst from above is evident. However, the coloured images also show black particles of calcined VPP that were never loaded into the reactor. It is unlikely that the calcined catalyst was exposed to temperatures greater than 760°C, which is thought to be the minimum temperature to drive the colour change. These changes are invisible to SEM or even SEM–EDX (as EDX is sensitive to atomic number but not the phase or oxidation state).

6 | CONCLUSIONS

The development of SEM has enabled researchers from a diverse range of scientific disciplines to image and analyze materials at high magnification and resolution. The technique is now commonplace and featured in many publications as a basic component of materials and solid matter research, particularly within the field of chemical engineering. The ability to visually check the morphology of nano-materials and observe changes post-use, for example, or following changes to synthesis variables, is invaluable when used in combination with other techniques that focus on the surface chemistries or bulk structure. The increased resolution of the more advanced systems (FEG-SEM) has broadened the applicability of this technique to look in more detail at nano-scale particulates, where previously this would have required TEM. However, tabletop SEM units are perfectly capable of resolving micro-structured materials and require little space compared to more advanced systems, increasing the technique's reach and appeal. The complimentary technique of XuM further develops the examination of micro-structured materials through the ability to generate X-ray-derived 3D tomographical representations.

ACKNOWLEDGEMENTS

The authors would like to thank Brendan A. Patience for collecting the original data set for the bibliometric map and generating the VOSViewer plot.

AUTHOR CONTRIBUTIONS

Thomas E. Davies: Data curation; formal analysis; investigation; visualization; writing – original draft; writing – review and editing. **He Li:** Conceptualization; data curation; formal analysis; investigation; methodology; validation; writing – original draft; writing – review and editing. **Stéphanie Bessette:** Data curation; formal analysis; investigation; methodology; writing – review and editing. **Raynald Gauvin:** Formal analysis; project administration; resources; supervision; validation; writing – original draft; writing – review and editing. **Gregory S. Patience:** Conceptualization; data curation; formal analysis; funding acquisition; investigation; methodology; project administration; resources; supervision; validation; writing – original draft; writing – review & editing. **Nicholas F. Dummer:** Conceptualization; data curation; formal analysis; investigation; methodology; resources; validation; visualization; writing – original draft; writing – review & editing.

DATA AVAILABILITY STATEMENT

We will make the data available to people that request it.

ORCID

Gregory S. Patience https://orcid.org/0000-0001-6593-7986

Nicholas F. Dummer https://orcid.org/0000-0002-0946-6304

REFERENCES

[1] Clarivate Analytics, Web of Science™ Core Collection **2021**, apps.webofknowledge.com (accessed: April 2021).

[2] H. Li, J. Li, J. Bodycomb, G. S. Patience, *Can. J. Chem. Eng.* **2019**, *97*, 1974.

[3] G. S. Patience, *Can. J. Chem. Eng.* **2018**, *96*, 2312.

[4] J. I. Goldstein, D. E. Newbury, P. Echlin, D. C. Joy, C. E. Lyman, E. Lifshin, L. Sawyer, J. R. Michael, *Scanning Electron Microscopy and X-Ray Microanalysis*, 3rd ed., Springer, Boston, MA **2003**, p. 21.

[5] T. Sunaoshi, K. Kaji, Y. Orai, C. T. Schamp, C. A. E. Voelkl, *Microsc. Microanal.* **2016**, *22*, 604.

[6] M. G. Rigamonti, Y.-X. Song, H. Li, N. Saadatkhah, P. Sauriol, G. S. Patience, *Can. J. Chem. Eng.* **2019**, *97*, 2251.

[7] H. Li, M. Rostamizadeh, K. Mameri, D. C. Boffito, N. Saadatkhah, M. G. Rigamonti, G. S. Patience, *Can. J. Chem. Eng.* **2019**, *97*, 2242.

[8] S. Liu, I. Gow, T. Davies, A. Barnes, M. Sankar, X. Gong, A. G. R. Howe, M. Dixon, G. J. Hutchings, C. J. Kiely, Q. He, *J. Mater. Chem. A* **2020**, *8*, 15725.

[9] D. C. Joy, *Monte Carlo Modeling for Electron Microscopy and Microanalysis*, Oxford University Press, Oxford **1995**.

[10] D. Wu, D. Gao, S. C. Mayo, J. Gotama, C. Way, *Compos. Sci. Technol.* **2008**, *68*, 178.

[11] T. E. Everhart, R. F. M. Thornley, *J. Sci. Instrum.* **1960**, *37*, 246.

[12] B. J. Griffin, *Scanning* **2011**, *33*, 162.

[13] H. Demers, N. Brodusch, D. C. Joy, P. Woo, R. Gauvin, *Microsc. Microanal.* **2013**, *19*, 364.

[14] P. G. Kotula, J. R. Michael, M. Rohde, *Microsc. Microanal.* **2008**, *14*, 116.

[15] D. Newbury, N. W. M. Ritchie, *J. Mater. Sci.* **2015**, *50*, 493.

[16] L. Reimer, *Scanning Electron Microscopy: Physics of Image Formation and Microanalysis*, 2nd ed., Springer, Berlin **2000**.

[17] A. Pakzad, N. Parikh, P. A. Heiden, R. S. Yassar, *J. Microsc.* **2011**, *243*, 77.

[18] J. I. Goldstein, D. E. Newbury, P. Echlin, D. C. Joy, C. E. Lyman, E. Lifshin, L. Sawyer, J. R. Michael, *Scanning Electron Microscopy and X-Ray Microanalysis*, 3rd ed., Springer, Boston, MA **2003**, p. 537.

[19] J. I. Goldstein, D. E. Newbury, P. Echlin, D. C. Joy, C. E. Lyman, E. Lifshin, L. Sawyer, J. R. Michael, *Scanning Electron Microscopy and X-Ray Microanalysis*, 3rd ed., Springer, Boston, MA **2003**, p. 565.

[20] N. J. van Eck, L. Waltman, *Scientometrics* **2010**, *84*, 523.

[21] M. An, Q. Guo, J. Ma, X. Hu, *Can. J. Chem. Eng.* **2020**, *98*, 1512.

[22] A. A. Barbosa, R. V. S. de Aquino, M. G. Silva, W. J. do Nascimento Júnior, M. M. M. B. Duarte, R. F. Dantas, O. R. S. da Rocha, *Can. J. Chem. Eng.* **2020**, *98*, 1124.

[23] B. Verma, C. Balomajumder, *Can. J. Chem. Eng.* **2020**, *98*, 2368.

[24] J. E. van den Reijen, S. Kanungo, T. A. J. Welling, M. Versluijs-Helder, T. A. Nijhuis, K. P. de Jong, P. E. de Jongh, *J. Catal.* **2017**, *356*, 65.

[25] Y. Takasu, N. Ohashi, X. G. Zhang, Y. Murakami, H. Minagawa, S. Sato, K. Yahikozawa, *Electrochim. Acta* **1996**, *41*, 2595.

[26] A. Chachvalvutikul, W. Pudkon, T. Luangwanta, T. Thongtem, S. Thongtem, S. Kittiwachana, S. Kaowphong, *Mater. Res. Bull.* **2019**, *111*, 53.

[27] J. McGlone, P. Priecel, L. D. Vià, L. Majdal, J. Lopez-Sanchez, *Catalysts* **2018**, *8*, 253.

[28] A. F. Sierra-Salazar, A. Ayral, T. Chave, V. Hulea, S. I. Nikitenko, S. Abate, S. Perathoner, P. Lacroix-Desmazes, *Unconventional Pathways for Designing Silica-Supported Pt and Pd Catalysts with Hierarchical Porosity*, Studies in Surface Science and Catalysis. Vol. 178, Elsevier, Amsterdam, The Netherlands **2019**, p. 377.

[29] M. Conte, C. J. Davies, D. J. Morgan, T. E. Davies, D. J. Elias, A. F. Carley, P. Johnston, G. J. Hutchings, *J. Catal.* **2013**, *297*, 128.

[30] T. J. Clarke, T. E. Davies, S. A. Kondrat, S. H. Taylor, *Appl. Catal. B-Environ.* **2015**, *165*, 222.

[31] P. M. Shah, A. N. Day, T. E. Davies, D. J. Morgan, S. H. Taylor, *Appl. Catal. B-Environ.* **2019**, *253*, 331.

[32] T. Weissenberger, B. Reiprich, A. G. F. Machoke, K. Klühspies, J. Bauer, R. Dotzel, J. L. Casci, W. Schwieger, *Catal. Sci. Technol.* **2019**, *9*, 3259.

[33] J. E. Blendell, *Solid State Sintering*, Elsevier, Amsterdam, The Netherlands **2001**, p. 8745.

[34] H. Abdelrazeq, P. Soboliak, M. A.-A. Al-Maadeed, M. Ouederni, I. Krupa, *Molecules* **2019**, *24*, 1217.

[35] D. Wei, J. G. Goodwin, R. Oukaci, A. H. Singleton, *Appl. Catal. A-Gen.* **2001**, *210*, 137.

[36] K. S. Choudhari, P. Jidesh, N. K. Udayashankar, *Synthesis and Reactivity in Inorganic Metal-Organic and Nano-Metal Chemistry* **2012**, *42*, 369.

[37] G. Wei, P. X. Ma, *Biomaterials* **2004**, *25*, 4749.

[38] A. Rabiei, A. G. Evans, *Acta Mater.* **2000**, *48*, 3963.

[39] T. Sekiguchi, T. Kimura, H. Iwai, *Superlattice. Microst.* **2016**, *99*, 165.

[40] T. Sun, L. Feng, X. Gao, L. Jiang, *Accounts Chem. Res.* **2005**, *38*, 644.

[41] C. G. Golding, D. R. B. L. L. Lamboo, T. F. Booth, *Sci. Rep.* **2016**, *6*, 26516.

[42] S. Zhang, F. Gelain, X. Zhao, *Semin. Cancer Biol.* **2005**, *15*, 413.

[43] S. Roffel, G. Wu, I. Nedeljkovic, M. Meyer, T. Razafiarison, S. Gibbs, *Clin. Implant Dent. R.* **2019**, *21*, 25.

[44] X.-B. Hu, Z. Chen, G. Tang, J.-L. Hou, Z.-T. Li, *J. Am. Chem. Soc.* **2012**, *134*, 8384.

[45] J. Mahamid, B. Aichmayer, E. Shimoni, R. Ziblat, C. Li, S. Siegel, O. Paris, P. Fratzl, S. Weiner, L. Addadi, *P. National Acad. Sci.* **2010**, *107*, 6316.

[46] M. F. Yu, O. Lourie, M. J. Dyer, K. Moloni, T. F. Kelly, R. S. Ruoff, *Science* **2000**, *287*, 637.

[47] A. Cao, P. L. Dickrell, W. G. Sawyer, M. N. Ghasemi-Nejhad, P. M. Ajayan, *Science* **2005**, *310*, 1307.

[48] D. J. Miller, C. Proff, J. G. Wen, D. P. Abraham, J. Bareño, *Adv. Energy Mater.* **2013**, *3*, 1098.

[49] F. Xu, Q. Qin, A. Mishra, Y. Gu, Y. Zhu, *Nano Res.* **2010**, *3*, 271.

[50] Z. J. Wang, G. Weinberg, Q. Zhang, T. Lunkenbein, A. Klein-Hoffmann, M. Kurnatowska, M. Plodinec, Q. Li, L. Chi, R. Schloegl, M. G. Willinger, *ACS Nano* **2015**, *9*, 1506.

[51] C. Kiely, G. Greenberg, C. J. Kiely, *Microsc. Microanal.* **2011**, *17*, 34.
[52] S. Meure, R. J. Varley, D. Y. Wu, S. Mayo, K. Nairn, S. Furman, *Eur. Polym. J.* **2012**, *48*, 524.
[53] N. F. Dummer, W. Weng, C. Kiely, A. F. Carley, J. K. Bartley, C. J. Kiely, G. J. Hutchings, *Appl. Catal. A-Gen.* **2010**, *376*, 47.
[54] A. C. Marques, H. Jain, C. Kiely, K. Song, C. J. Kiely, R. M. Almeida, *J. Sol-Gel Sci. Techn.* **2009**, *51*, 42.
[55] F. H. She, D. Gao, W. M. Gao, D. Y. Wu, Z. Peng, M. Hoang, L. X. Kong, *Desalination* **2009**, *236*, 179.
[56] H. Li, A. Ndjamo, P. Sauriol, G. S. Patience, *Adv. Powder Technol.* **2017**, *28*, 1000.
[57] B. J. Griffin, *Methods in Molecular Biology* **2007**, *369*, 467.
[58] N. Braidy, A. Béchu, J. C. de Souza Terra, G. S. Patience, *Can. J. Chem. Eng.* **2020**, *98*, 628.
[59] S. Badehbakhsh, N. Saadatkhah, M. J. D. Mahboub, O. Guerrero-Pérez, G. S. Patience, *Catal. Today* **2021**. https://doi.org/10.1016/j.cattod.2021.12.008

How to cite this article: T. E. Davies, H. Li, S. Bessette, R. Gauvin, G. S. Patience, N. F. Dummer, *Can. J. Chem. Eng.* **2022**, 1. https://doi.org/10.1002/cjce.24405